



DFT and PIO study of the influences of Mo valence state and surface hydroxyl on supported-MoO_x catalysts for ethylene polymerization

Xiaochun Cao, Ruihua Cheng*, Zhen Liu, Lisong Wang, Qi Dong, Xuelian He, Boping Liu*

State Key Laboratory of Chemical Engineering, East China University of Science and Technology, Meilong Road 130, Shanghai 200237, PR China

ARTICLE INFO

Article history:

Received 11 November 2009

Received in revised form 10 January 2010

Accepted 26 January 2010

Available online 2 February 2010

Keywords:

Supported-MoO_x catalyst
Ethylene polymerization
Molecular modeling
Valence state
Surface hydroxyl

ABSTRACT

Phillips catalyst (CrO_x/SiO₂) is an important industrial catalyst for ethylene polymerization, but the highly toxic chromium may contaminate the environment and do harm to human's health. Supported-MoO_x catalyst with low toxicity has potential to replace Phillips catalyst if its catalytic performance could be improved. In this work, models of molybdenum active sites with different valence states (5+, 4+, 3+, 2+) supported on Al₂O₃ and SiO₂, respectively, were established to investigate the effects of the valence states and surface hydroxyl on the catalyst activity using the combination of density functional theory (DFT) and paired interacting orbitals (PIO) methods. DFT results showed that supported Mo²⁺ center had the lowest energy barrier of ethylene insertion and thus possessed the highest activity for ethylene polymerization. PIO method additionally elucidated the orbital interaction and electron transformation between Mo²⁺ center and ethylene monomer. Hydroxyl on the support surface could poison the active center by coordination with Mo center. It had been demonstrated that pre-reduction of hexa-valent molybdenum into lower valence state +2 and elimination of surface hydroxyl groups of support were the key factors to obtain highly efficient ethylene polymerization catalyst. The molecular modeling results of this work provided theoretical basis for further experimental developments of green and highly efficient supported Mo-based polyethylene catalysts.

© 2010 Elsevier B.V. All rights reserved.

1. Introduction

Phillips catalyst (CrO_x/SiO₂), which was discovered by Hogan and Banks in Phillips Petroleum Company in the early 1950s, is unique among industrial polyethylene catalysts due to its unique microstructures of polymer products with ultra-broad molecular weight distribution and long chain branches [1,2]. Nowadays, Phillips catalyst is still used in many industrial ethylene polymerization processes and is producing about 40–50% world's high density polyethylene (HDPE) which played very important role in human's daily life and various industrial applications. However, the high toxicity of Phillips catalyst is still remained as a great challenge in this field.

Phillips catalyst was originally prepared with highly toxic CrO₃. Later on, a lot of efforts had been devoted in substituting CrO₃ with much less poisonous chromate (III) acetate [3–5] to meet the increasing demands from environmental and health considerations. But the obtained catalyst from chromate (III) acetate after calcination was still in the form of highly toxic hexa-valent chromate species. Moreover, Cr-containing waste water and solid dust

produced during catalyst preparation, and Cr residues in polyethylene products could still possibly contaminate environment and threaten human's health as well. Increasing concern and strict environmental regulations required us to further seek a greener catalyst as a complete substitution of Cr-based Phillips catalyst in the future.

As an environmentally friendly catalyst, supported molybdenum oxide catalyst had been reported to be active for olefin polymerization long time before. As early as in 1950s, Indiana Standard Oil Company [6] had discovered the ethylene polymerization catalyst based on molybdenum oxides. The effects of preparation conditions, solvent and ratio of molybdenum to metal hydride on the performance of MoO_x/Al₂O₃ catalyst for ethylene polymerization were further reported in the 1954s patent [7]. This Mo-based catalyst technology was first adopted by a Japanese company for commercial polyethylene production in 1961. Consequently, this process was dumped out because of its poor catalytic performance. Our preliminary experimental result with MoO_x/SiO₂ catalyst was also found to be active for ethylene polymerization, but the activity was low. If the catalytic performance of supported molybdenum oxide catalyst could be improved to the level of Phillips catalyst, a complete substitution of Cr-based Phillips catalyst with Mo-based catalyst could be plausible in the near future. Chromium and molybdenum both belong to group 6 B in the Periodic Table, and the precursors of supported MoO_x and CrO_x

* Corresponding authors. Tel.: +86 21 64253627; fax: +86 21 64253627.

E-mail addresses: rhcheng@ecust.edu.cn (R. Cheng), boping@ecust.edu.cn (B. Liu).

catalysts were also with similar surface structure (shown in Fig. 1). Thus supported molybdenum oxide catalyst as well as Phillips catalyst could all catalyze ethylene polymerization possibly following a similar mechanism. This inspired us to further study the supported molybdenum oxides catalyst for ethylene polymerization in detail.

In order to develop newly green and highly efficient Mo-based catalyst for ethylene polymerization, it is very important to clarify the mechanism first, which may provide some theoretical guidance for further practical experimental exploration. For heterogeneous supported-MoO_x catalyst, the valence state of molybdenum active site was still ambiguous and hydroxyl on the support surface may also be involved in the reaction. Thus this work will focus on the effects of Mo valence state and surface hydroxyl on the ethylene polymerization activity of supported-MoO_x catalysts.

MoO₃/Al₂O₃ catalyst was also found to be active for olefin metathesis in 1956s [8]. The performance of MoO₃/Al₂O₃ catalyst for olefin metathesis had been well studied both experimentally [9–12] and theoretically [13,14]. Except a few experimental reports, no theoretical investigation on olefin polymerization over supported-MoO_x catalyst could be found in the literature. In recent decades, quantum chemical methods like DFT and PIO are becoming more and more important for molecular level investigation of various supported catalytic systems.

Bao and co-workers [13] established two different molybdenum active sites of Mo^{VI}O₂ and Mo^VO(OH) over the Mo/HBeta catalytic systems applying DFT method, and reported that the Mo^{VI} active site was more efficient in catalyzing the formation of Mo-methylidene species than Mo^V active site. Handzlik and Ogonowski [14] used DFT method to study ethylene metathesis over the MoO_x/Al₂O₃ catalyst and showed that the active centers for ethylene metathesis may contain Mo^{VI} rather than Mo^{IV}. PIO method, which was developed by Fujimoto et al. [15] based on the frontier orbital theory of Fukui et al. [16], was very powerful to analysis of the orbitals interaction and electronic transformation in catalytic reactions. Handzlik et al. [17] found that the total overlap population was a useful reactivity index for the Mo-based olefin metathesis catalysts. On other systems, Shiga et al. [18] studied the effect of ligands in the methyltitanium complexes on ethylene insertion into the Ti–C bond using PIO method, and found electron delocalization was from the methyltitanium compound to ethylene firstly, and then ethylene to methyltitanium compound. Liu et al. [19] applied PIO method combined with DFT calculation to investigate the intermolecular orbital interactions between ethylene monomer and a molecular model of surface mono-chromate species for Phillips catalyst. Thus, computer modeling simulation was an efficient way to study the valence state of active site, the molecular interaction and electronic transformation over supported Mo-based catalyst. In the present work, modeling simulation based on DFT method was used to investigate the influences of active oxidation state of molybdenum and surface hydroxyl on the polymerization activity of supported Mo-based catalysts. PIO method was used additionally to investigate the orbitals interaction and electron transformation between Mo active center and coordinating ethylene monomer. It was expected that the study could provide some theoretical guidance for further exploitation of environmentally friendly

supported-MoO_x catalyst with high performance for ethylene polymerization.

2. Experimental and computational methods

2.1. Experimental method

2.1.1. Preparation of catalyst

SiO₂-supported-MoO_x catalyst was prepared by impregnating water solution of (NH₄)₆Mo₇O₂₄·4H₂O (AR, purchased from Sinopharm Chemical Reagent Co.) on SiO₂ (Grace Davison 955 with BET surface area ca. 270.4 m²/g, donated by Qilu Branch Co., SINOPEC) for 4 h at room temperature, and then dried at 110 °C for 6 h, followed by a calcination process. The calcination was performed in a quartz fluidized bed at high purity air atmosphere with a flow rate of 600 mL/min at 600 °C for 5 h. In this way, a MoO_x/SiO₂ catalyst with 8 wt.% of Mo loading was obtained and stored in the glove box before using.

2.1.2. Ethylene polymerization over MoO_x/SiO₂ catalyst

Before polymerization, ethylene (polymerization grade, purchased from Chunyu Special Gas Co.) was purified by passing through a 4A molecular sieve column, a Copper oxide catalyst column and a 13X molecular sieve column to further remove moisture and oxygen impurities. The polymerization conditions were shown as follows: ethylene pressure 0.15 MPa, polymerization temperature: 90 °C, solvent: 70 mL n-heptane purified by distillation after drying over sodium metal (AR, purchased from Shanghai Experiment Reagent Co.). Co-catalyst: aluminum triisobutyl (TIBA, 25% w/w in hexane, 95%, purchased from Alfa Aesar). The polymerization was terminated by adding 50 mL ethanol/HCl solution after 1 h. The polymer was washed and dried in vacuum at 60 °C for 4 h.

2.1.3. Polymer characterization

The obtained polymer was characterized using differential scanning calorimetry (DSC, Pyris Diamond) under nitrogen atmosphere. The sample was scanned according to the following four steps: (i) heated from room temperature to 150 °C at a rate of 10 °C/min; (ii) held at 150 °C for 5 min; (iii) cooled to the room temperature at a rate of 10 °C/min; (iv) repeated the first step again. Fourier transform infrared spectroscopy (FTIR, NICOLET 5700) method was used to confirm the polyethylene obtained.

2.2. Computational method

In this work, ethylene polymerization over supported molybdenum oxide catalyst was studied through a theoretical approach in combination of DFT and PIO methods.

Calculations were carried out with the Gaussian 03 program [20]. DFT method and B3LYP functional, which contained 20% of Hartree–Fock exchange and combined Becke's exchange [21,22] and Lee, Yang and Parr's correlation functional [23], were applied to optimize the neutral geometric structures of reactants and products without symmetry constraints. The Gibbs free energy of each equilibrium geometry was obtained at gas phase, 298.15 K and 1 atmospheric pressure. Each reactant and product pair with minimum Gibbs free energy was used to search for the transition state, which was verified by IRC calculations [24,25]. Frequency calculations were all carried out to ensure that all the stationary points (reactant and product) possessed no imaginary vibrations and each transition state possessed only one imaginary vibration. Mo centers with low valence states possessed several possible spin multiplicities, for instance, Mo⁴⁺: singlet and triplet, Mo³⁺: doublet and quartet, Mo²⁺: singlet, triplet and quintet. Confirmation of the ground spin state for each Mo center in different oxidation state is the most important thing and had been done first. It was confirmed

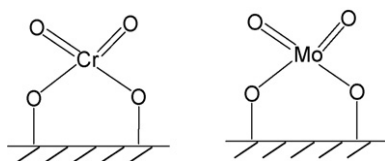


Fig. 1. Precursors of supported CrO₃ and MoO₃ catalysts.

that the ground spin state of Mo^{5+} , Mo^{4+} , Mo^{3+} and Mo^{2+} centers were doublet, triplet, quartet and quintet, respectively. (These calculation results could be found in the supporting information.) The LANL2DZ basis set with relativistic effective core potential (RECP) of Hay and Wadt [26] was used to describe the Mo element, and the 6-31G (d, p) basis set was applied for C, H, O, Al, Si atoms. The Mulliken charge of molybdenum atom was also calculated by Gaussian 03 program for analysis of the charge distribution on each center.

PIO method, which was proposed by Fujimoto et al. [15] based on the frontier orbital theory of Fukui et al. [16], was very powerful to analyze the orbitals interaction and electronic transformation in catalytic reactions. It has been proven to be mostly useful for studies on transition metal-contained complex system. In this work, LUMMOX software developed by Sumitomo Chem. Corp based on the PIO theory was used to analyze the orbitals interaction and electronic transformation between Mo center and ethylene monomer. The molecular orbital calculations by PIO were based on the extended Hückel methodology. The Cartesian coordinates of molecular models for PIO calculations were obtained from DFT results.

3. Results and discussion

3.1. Experimental results

In this work, Al/Mo molar ratio was changed from 2.5 to 30 to explore the optimum condition for the highest activity of $\text{MoO}_x/\text{SiO}_2$ catalyst for ethylene polymerization. The results showed that the highest catalyst activity of $2.4 \text{ g}_{\text{polymer}}/\text{g}_{\text{cat}}/\text{h}$ was obtained at Al/Mo=5. Fig. 2 shows the DSC and FTIR profiles of the polymer produced over the $\text{MoO}_x/\text{SiO}_2$ catalyst. DSC profile showed the melting point of the polymer was 134.8°C , which suggested the polymer might be polyethylene. FTIR measurement of the obtained polymer was carried out for further confirmation. The typical FTIR symmetry and anti-symmetry vibration frequency of CH_2 group at 2848 cm^{-1} and 2920 cm^{-1} , respectively, further proved the polymer was polyethylene. Thus, $\text{MoO}_x/\text{SiO}_2$ catalyst was confirmed to be active for ethylene polymerization although the activity was relatively low. As for $\text{MoO}_x/\text{Al}_2\text{O}_3$ catalyst, it was also reported to be active for ethylene polymerization [7]. The activity of $\text{MoO}_x/\text{Al}_2\text{O}_3$ catalysts for ethylene polymerization was $179 \text{ g}_{\text{polymer}}/\text{g}_{\text{cat}}/\text{h}$, which was much higher than that of the $\text{MoO}_x/\text{SiO}_2$ catalyst prepared in this work. According to our DFT calculation results which will be shown in the following sections, $\text{MoO}_x/\text{SiO}_2$ model catalysts even showed a bit higher polymerization activity (a bit lower energy barrier of ethylene insertion) compared with that of $\text{MoO}_x/\text{Al}_2\text{O}_3$ model catalysts. This discrepancy mainly derived from the difference of catalyst preparation process and polymerization reaction conditions applied for the two catalyst systems. As for $\text{MoO}_x/\text{Al}_2\text{O}_3$ catalyst, pre-reduction was carried out with dry H_2 at 480°C for 16 h. Ethylene polymerization was carried out under 256°C and 6.0 MPa. Xylene and CaH_2 were also added to the reactor as the solvent and co-catalyst, respectively. As for $\text{MoO}_x/\text{SiO}_2$ catalyst, it was used for ethylene polymerization at 90°C and 0.15 MPa without catalyst pre-reduction, n-heptene and TIBA were used as the solvent and co-catalyst, respectively. It was concluded that $\text{MoO}_x/\text{Al}_2\text{O}_3$ and $\text{MoO}_x/\text{SiO}_2$ catalyst were all active for ethylene polymerization, but a direct comparison of these two catalyst systems was quiet difficult up to now, which need further experimental confirmation. In order to develop green and highly efficient Mo-based polyethylene catalysts, the corresponding models of $\text{MoO}_x/\text{Al}_2\text{O}_3$ and $\text{MoO}_x/\text{SiO}_2$ catalysts were established in the following computational modeling work to investigate the effects of Mo valence state and surface hydroxyl on the polymerization activity.

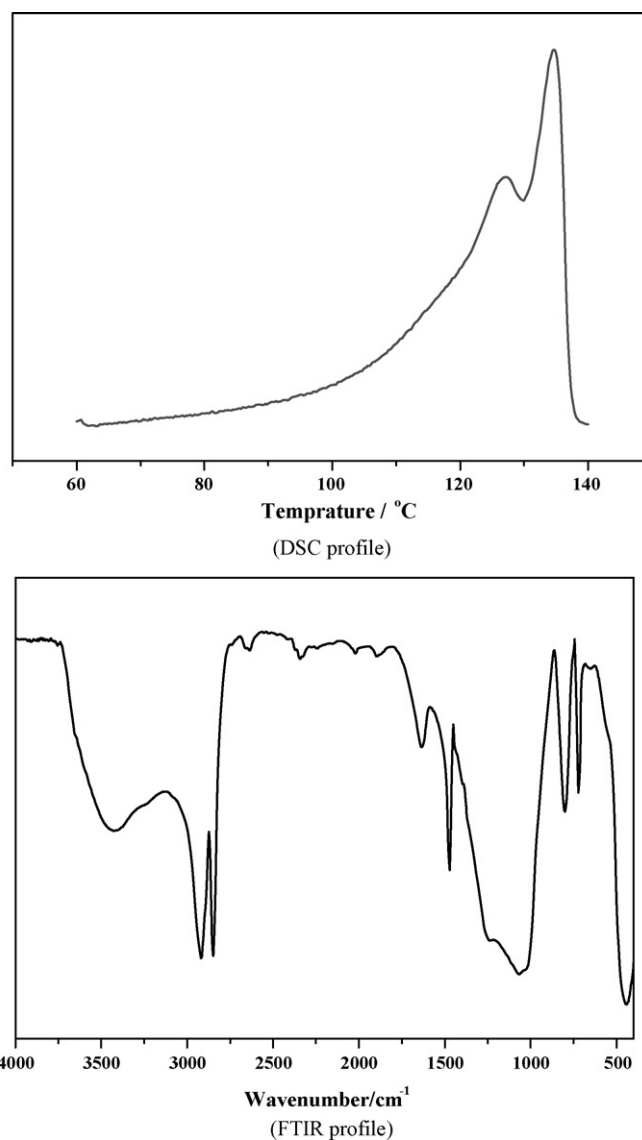


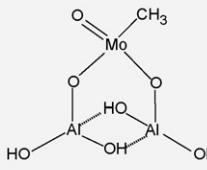
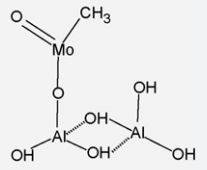
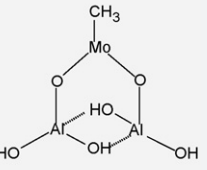
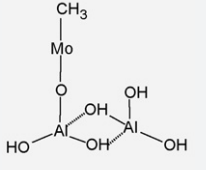
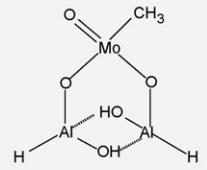
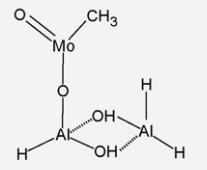
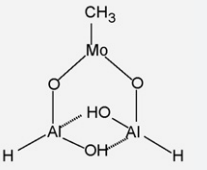
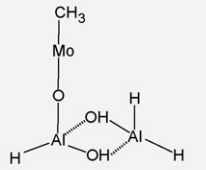
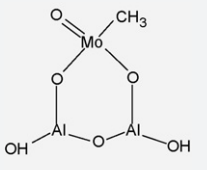
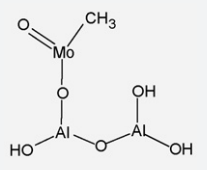
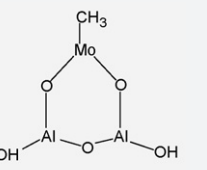
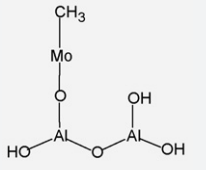
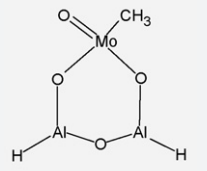
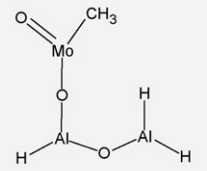
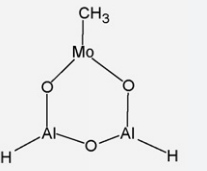
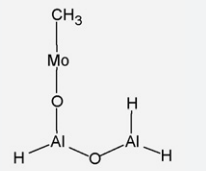
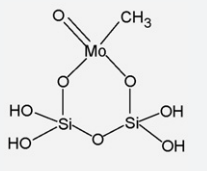
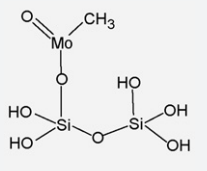
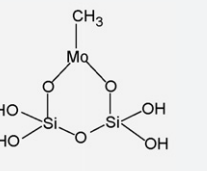
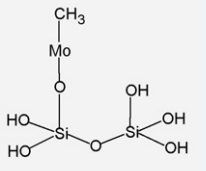
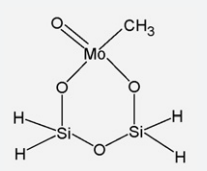
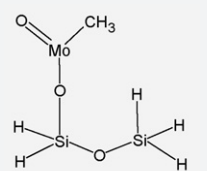
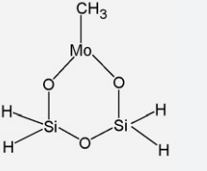
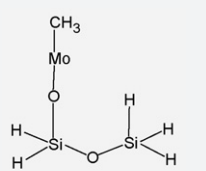
Fig. 2. DSC and FTIR profiles of the polymer produced by $\text{MoO}_3/\text{SiO}_2$ catalyst (the catalyst residue was not removed from the polymer).

3.2. Computational modeling of supported Mo-based catalysts

As the literature reported [27], when molybdenum content was very low, Mo species mainly existed in an isolated form on the catalyst surface. In the present work, four kinds of isolated molybdenum site models with different valence states were established. According to Cossee mechanism [28], the metal-C center was proposed as the active site for olefin polymerization. The growing polymer chain was simplified as a methyl group. So here, except for Mo-C bond, the number of oxygen linked with molybdenum in the form of $\text{Mo}=\text{O}$ or $\text{Mo}-\text{O}$ was adjusted to obtain a set of neutral mononuclear Mo active centers with the oxidation states of +5, +4, +3, +2, respectively. For instance, Mo^{5+} model contained one Mo-C single bond, one $\text{Mo}=\text{O}$ double bond and two Mo-O single bonds bridging to the support model; Mo^{4+} model contained one Mo-C, one $\text{Mo}=\text{O}$ and one Mo-O single bond anchoring to the support model; Mo^{3+} model with one Mo-C and two Mo-O single bonds attaching to the support model; and Mo^{2+} model with one Mo-C and one Mo-O single bond linking to the support surface. The structures of Mo^{4+} model and Mo^{2+} model were mononuclear Mo center supported on the Al_2O_3 and SiO_2 through single Mo-O-Al and Mo-O-Si bridges, respec-

tively, which was different with Mo^{5+} and Mo^{3+} models including double bridges. For Mo^{4+} model, double-bridged structure would lead to much more different dinuclear Mo center. As for Mo^{2+} model, only single bridge is possible. Such Cr-based SiO_2 -supported catalyst through single Si–O–Cr bridge for ethylene trimerization had been reported experimentally [29,30]. The bond length of Mo=O and Mo–O in these models were about 1.70 Å and 1.96 Å, respectively, which was in accordance with the EXAFS results that the bond length of Mo=O and Mo–O in the $\text{MoO}_4\text{Si}_2\text{O}_2(\text{OH})_2$ catalyst model were 1.69 Å and 2.00 Å, respectively [31]. Thus Mo site models with different valence states were established.

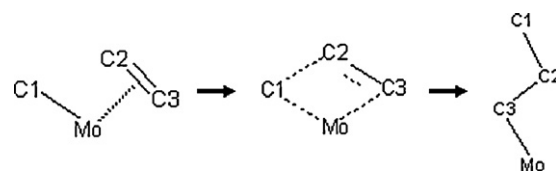
Table 1
Mo active site models with different valence states supported on Al_2O_3 or SiO_2 .

Models	Mo^{5+}	Mo^{4+}	Mo^{3+}	Mo^{2+}
$\text{MoO}_x\text{-Al}_2(\text{OH})_2(\text{OH})_y$ a	 5a	 4a	 3a	 2a
$\text{MoO}_x\text{-Al}_2(\text{OH})_2\text{H}_y$ b	 5b	 4b	 3b	 2b
$\text{MoO}_x\text{-Al}_2\text{O}(\text{OH})_y$ c	 5c	 4c	 3c	 2c
$\text{MoO}_x\text{-Al}_2\text{OH}_y$ d	 5d	 4d	 3d	 2d
$\text{MoO}_x\text{-Si}_2\text{O}(\text{OH})_y$ e	 5e	 4e	 3e	 2e
$\text{MoO}_x\text{-Si}_2\text{OH}_y$ f	 5f	 4f	 3f	 2f

As for the modeling of the support, this work selected two widely used molecular cluster models of supports Al_2O_3 and SiO_2 . These models were mainly referred from the literature. As for Al_2O_3 support, Handzlik et al. [14,32] studied the effect of Al atom number on performance of $\text{MoO}_x/\text{Al}_2\text{O}_3$ catalyst for ethylene metathesis, and found that a molecular cluster with two alumina atoms could be a good model of the Al_2O_3 support. As for SiO_2 support, Hierl and Krauss [33], working from gravimetric measurement study by CO reduction, concluded that chromate (one chromium atom attached to two silicon atoms through two oxygen bridges) was the dominant species. Similar models of SiO_2 was also used by Espelid et al.

[34] to construct a mononuclear Cr(II) sites cluster model of Phillips catalyst to investigate the initiation and chain propagation mechanisms. Scott and co-worker recently confirmed the validation of these chromasiloxane models [35]. Thus, cluster models of Al_2O_3 with two alumina atoms and cluster models of SiO_2 with two silicon atoms were selected for the DFT calculations in this work.

In summary, molybdenum centers with different valence state were attached to the support models of Al_2O_3 or SiO_2 through Mo–O–Al or Mo–O–Si linkages. All the catalyst models are shown in Table 1. $\text{MoO}_x\text{-Al}_2(\text{OH})_2(\text{OH})_y$ (**a**) and $\text{MoO}_x\text{-Al}_2(\text{OH})_2\text{H}_y$ (**b**) represented molybdenum centers attached to two Al atoms that were bridged by two coordinated hydroxyl groups. $\text{MoO}_x\text{-Al}_2\text{O}(\text{OH})_y$ (**c**) and $\text{MoO}_x\text{-Al}_2\text{OH}_y$ (**d**) were the simplified models of **a** and **b** with one H_2O molecule eliminated, and two Al atoms were connected by one oxygen atom. Models of $\text{MoO}_x\text{-Si}_2\text{O}(\text{OH})_y$ (**e**) and $\text{MoO}_x\text{-Si}_2\text{OH}_y$ (**f**) represented molybdenum centers attached to two Si atoms that were connected by one oxygen atom. Here, Mo^{5+} , Mo^{4+} , Mo^{3+} , Mo^{2+} centers for model catalyst **a** were represented as **5a**, **4a**, **3a**, **2a**, respectively, TS was the transition state, and **5ap**, **4ap**, **3ap**, **2ap** were their corresponding products after ethylene insertion. The other catalyst models (**b**, **c**, **d**, **e**, **f**) in different valence state,



Scheme 1. Chain propagation according to Cossee mechanism.

TSs and products before and after ethylene insertion were named similar to those of model **a**. For all cluster models, the required valence for the support atoms (four for Si and three for Al) were saturated by the appropriate number of hydroxyl (OH) groups or H atoms, which stands for fully hydroxylated or dehydroxylated support surface, respectively.

3.3. Effects of Mo valence state on catalyst activity

The valence state of transition metal active site might change during reaction, which made the mechanism research very complicated. In order to accomplish the complete substitution of highly toxic Cr-based Phillips catalyst by green Mo-based catalyst, it was

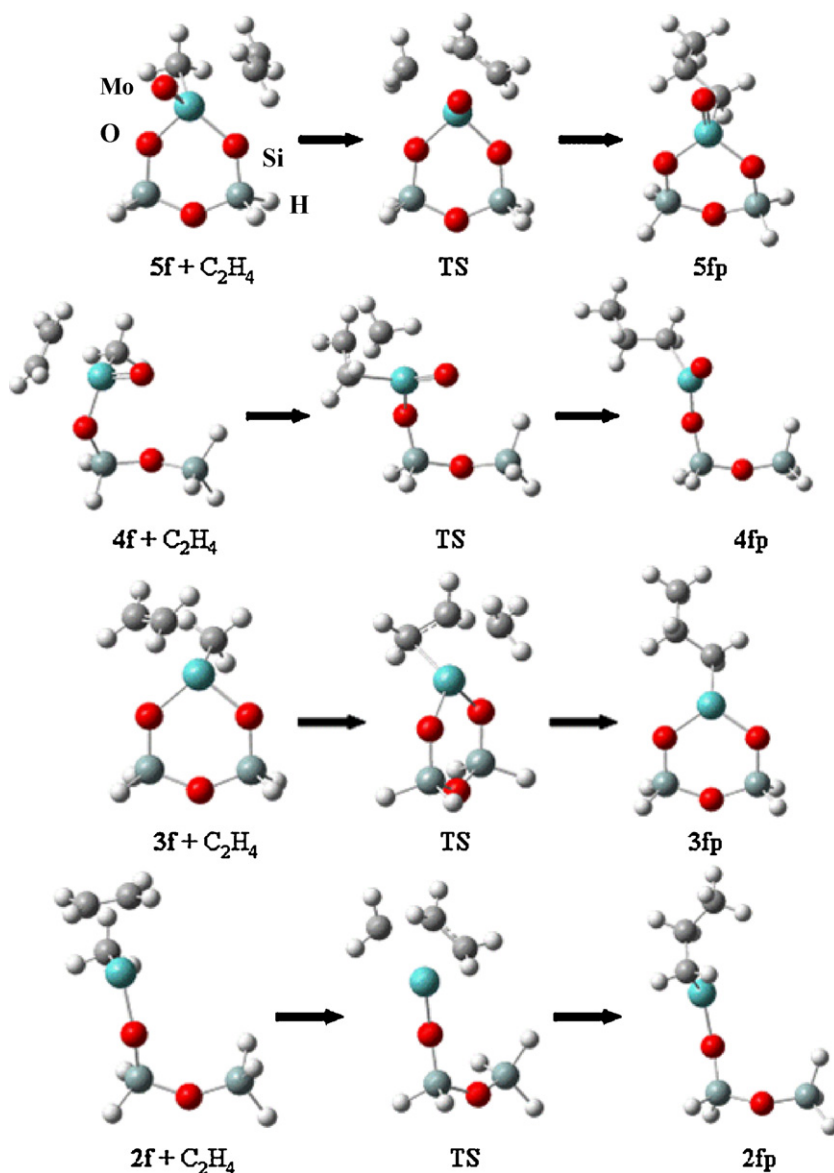


Fig. 3. Reaction pathways of ethylene insertion into molybdenum centers with different valence states (**5f**, **4f**, **3f** and **2f**) for $\text{MoO}_x\text{-Si}_2\text{OH}_y$ catalysts.

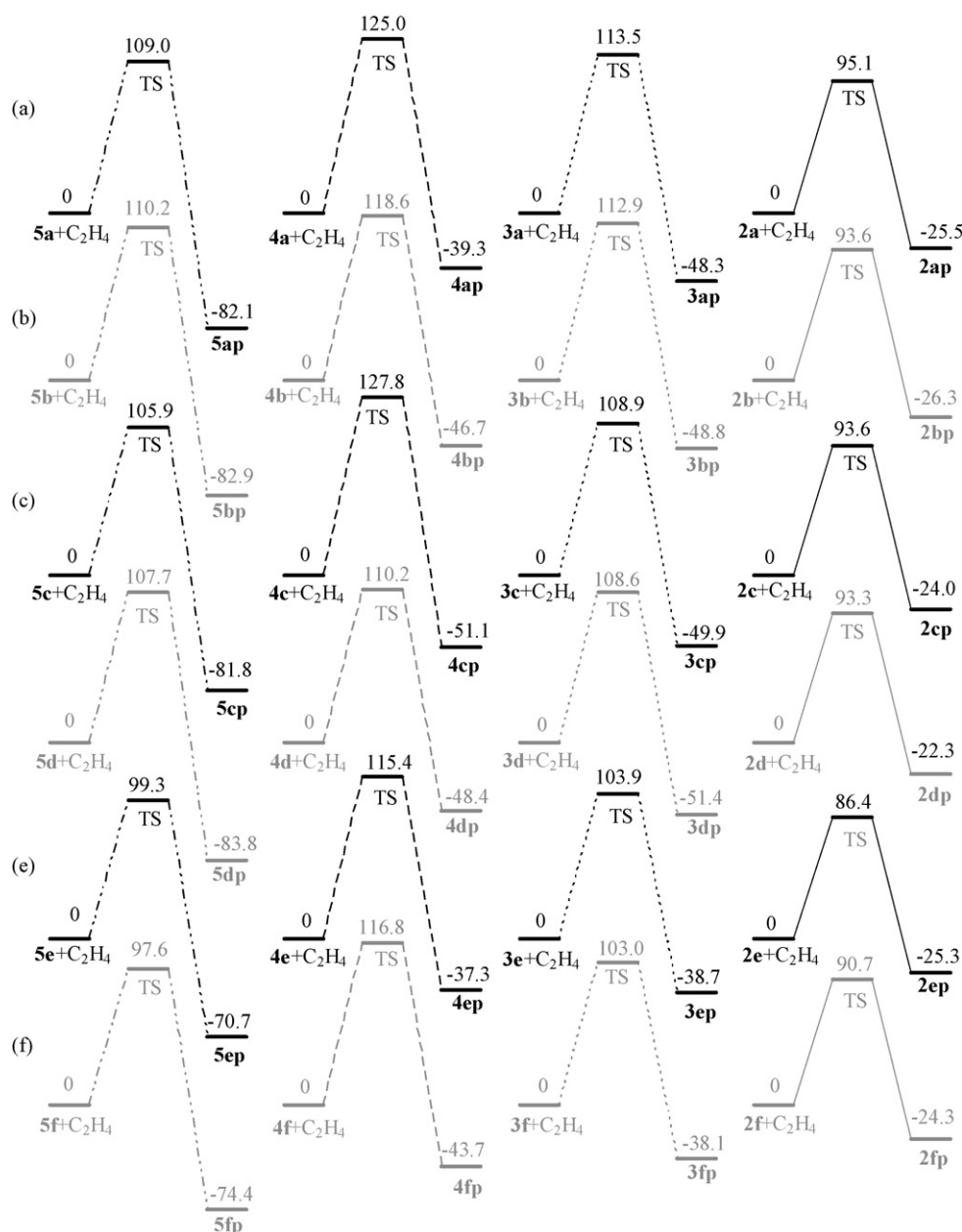


Fig. 4. Energy profiles of ethylene insertion into different supported catalyst models. **a**, $\text{MoO}_x\text{-Al}_2(\text{OH})_2(\text{OH})_y$; **b**, $\text{MoO}_x\text{-Al}_2(\text{OH})_2\text{H}_y$; **c**, $\text{MoO}_x\text{-Al}_2\text{O}(\text{OH})_y$; **d**, $\text{MoO}_x\text{-Al}_2\text{OH}_y$; **e**, $\text{MoO}_x\text{-Si}_2\text{O}(\text{OH})_y$; **f**, $\text{MoO}_x\text{-Si}_2\text{OH}_y$ (energy in kJ/mol). The energies of transition state (TS) and product of each model were referenced to each active site model coordinated with ethylene.

very important to clarify the valence state of Mo active site for ethylene polymerization to establish a theoretical basis for further experimental exploration of Mo-based polyethylene catalyst with high performance.

As the ethylene insertion process according to Cossee mechanism showed in Scheme 1, ethylene inserted into the active center accompanied with the breaking of Mo–C1 bond, followed by a regeneration of the active site through formation of a new bond between the C3 in ethylene and Mo active center. So during the ethylene insertion process through a transition state from reactant to product, Mo–C1 bond became longer, and C3 would be stretched closer to the Mo center. At the same time, distance between C2 and C1 became also shorter than before. For instance, bond changes during ethylene insertion into 2f model was described as follows: First, the distance between Mo and C1 was 2.15 Å, which was stretched to 2.34 Å in the transition state, and the final distance between Mo and

C1 atoms was 3.69 Å, indicating of complete breaking of the original Mo–C1 bond. With the increasing length of Mo–C1 bond, the distance between Mo and C3 atoms became shorter, which changed from 2.49 Å to 2.19 Å from coordination state to transition state, and the length of newly formed Mo–C3 bond in the product 2fp was 2.13 Å. At the same time, there would regenerate another new bond between C1 and C2, which has changed from 3.26 Å to 2.11 Å from coordination state to transition state, the formed C1–C2 bond in the final product 2fp was 1.53 Å. Taking f models as an example, the reaction pathways of ethylene insertion into molybdenum centers with different valence states (5f, 4f, 3f and 2f) were shown in Fig. 3.

The energy barriers of ethylene insertion into Mo centers with different valence states supported on Al_2O_3 or SiO_2 are shown in Fig. 4. It was also noted that ethylene insertion energy barrier for SiO_2 -supported catalysts were a little bit lower than that of

Table 2
Atomic distance (Å) between Mo and C1 before or after the ethylene coordination for the Mo-based catalyst models.

Model	Mo–C1 ^a	Mo–C1 ^b	Model	Mo–C1 ^a	Mo–C1 ^b
5a	2.13	2.15	5b	2.13	2.15
4a	2.13	2.13	4b	2.13	2.13
3a	2.13	2.14	3b	2.13	2.14
2a	2.13	2.16	2b	2.13	2.16
5c	2.13	2.14	5d	2.13	2.14
4c	2.12	2.13	4d	2.11	2.12
3c	2.13	2.13	3d	2.13	2.13
2c	2.13	2.15	2d	2.12	2.15
5e	2.12	2.14	5f	2.12	2.14
4e	2.12	2.13	4f	2.13	2.14
3e	2.11	2.12	3f	2.12	2.12
2e	2.11	2.14	2f	2.12	2.15

^a Catalyst before ethylene coordination.

^b Catalyst after ethylene coordination.

Al₂O₃-supported ones. However, for the same kind of support, the energy barriers were sensitive to the valence states of Mo centers, and the models employed here all followed the same principle: Mo⁴⁺ models represented the highest ethylene insertion energy barrier, and the Mo²⁺ models presented the lowest ethylene insertion energy barrier. Here, series of **d** models (MoO_x-Al₂OH_y) were taken as an example for Al₂O₃-supported Mo-based catalysts. The energy barrier of ethylene insertion increased from 107.7 kJ/mol for **5d** model to 110.2 kJ/mol for **4d** model, and then decreased to 108.6 kJ/mol for **3d** model. The **2d** model presented the lowest energy barrier of 93.3 kJ/mol for ethylene insertion. Series of **f** models (MoO_x-Si₂OH_y) were also taken as an example for SiO₂-supported Mo-based catalysts. The energy barriers of ethylene insertion were 97.6 kJ/mol for **5f** model, 116.8 kJ/mol for **4f** model, and 103.0 kJ/mol for **3f** model. For the case of **2f** model, it also presented the lowest energy barrier of 90.7 kJ/mol for ethylene insertion. The general tendency of the increasing of polymerization activity on Mo valence state for all six types of catalyst models was found to be as follows: Mo⁴⁺ < Mo³⁺ < Mo⁵⁺ < Mo²⁺. These molecular modeling results suggested that the divalent oxidation state might be the real oxidation state of the Mo active site for both MoO_x/Al₂O₃ and MoO_x/SiO₂ catalysts for ethylene polymerization.

The dependence of activity on valence state for all six types of catalyst models: Mo⁴⁺ < Mo³⁺ < Mo⁵⁺ < Mo²⁺ could be rationalized as follows. For coordination polymerization, coordination of ethylene monomer is an important step for the subsequent insertion and propagation reaction. At the coordination state, the coordinated ethylene plays the important role of elongating and weakening the Mo–C1 bond of the active sites facilitating the subsequent insertion. If the Mo–C1 bond elongated most obviously after ethylene coordination, it could weaken the Mo–C1 bond through reducing the electronic density between Mo and C1 regions and thus decrease the insertion energy barrier for the subsequent ethylene insertion step. As shown in Table 2, the Mo–C1 bond all elongated after ethylene coordination for all six kinds of supported catalyst models. Generally, after ethylene coordination the Mo–C1 bond elongation order was obtained as follows: Mo²⁺ > Mo⁵⁺ > Mo³⁺ ≈ Mo⁴⁺, which was consistent with the activity order as described above. The prolongation of Mo–C1 bond in Mo²⁺ models were the most obvious after ethylene coordination compared with the Mo⁵⁺, Mo⁴⁺ and Mo³⁺ models, which was in consistence with the result discussed above that Mo²⁺ possessed the lowest ethylene insertion energy barrier. Take **d** model as an example for the MoO_x/Al₂O₃ catalyst, the change of Mo–C1 bond of **2d** model was most obviously, which was elongated from 2.12 Å to 2.15 Å after ethylene coordination. So ethylene inserted into Mo–C1 in **2d** model most easily. As for the **4d** model, the smallest change

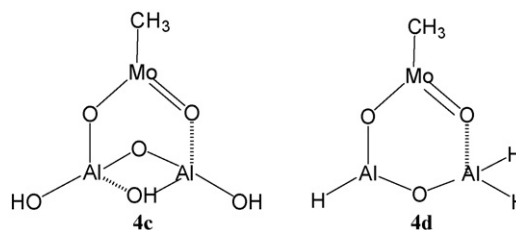


Fig. 5. Coordination of oxo atom in Mo=O double bond with aluminum atom on the Al₂O₃ support for the **4c** and **4d** models.

of Mo–C1 bond length (from 2.11 Å to 2.12 Å) could be observed after ethylene coordination. The **f** model was taken as an example for the MoO_x/SiO₂ catalyst. It showed that the Mo–C1 bond of **2f** model also changed most obviously after ethylene coordination, which was elongated from 2.12 Å to 2.15 Å. So ethylene inserted into Mo–C1 of **2f** model most easily. As for the **4f** model, the Mo–C1 bond length also showed the smallest change (2.13–2.14 Å) after ethylene coordination.

An interesting phenomenon for **4c** and **4d** models supported on Al₂O₃ was found that the oxo in Mo=O double bond could coordinate with the aluminum atom on the support surface (as shown in Fig. 5). For **4c** model, the coordination between oxo and aluminum converted the Al₂O₃ configuration with two aluminum atoms connected by one oxygen atom into more stable bridged structure similar to **4a** model. The geometry of **4d** model would be much similar with that of **3d** model after the coordination between oxo with aluminum. This might contribute to the strong coordination ability of aluminum atom, which could not be found for the **4e** and **4f** models supported on SiO₂. However, such coordination of oxo with aluminum atom in the Al₂O₃ support did not change its highest ethylene insertion energy barrier for Mo⁴⁺ sites among all the oxidation states.

It could be concluded that supported Mo²⁺ catalyst model presented the lowest energy barrier for ethylene insertion, and was thought to be the real oxidation state of active site for ethylene polymerization over both MoO_x/Al₂O₃ and MoO_x/SiO₂ catalysts. The molybdenum centers with higher valence states (from +4 to +6) were usually reported as the active site for Mo-catalyzed olefin metathesis [14], thus it would be efficient to enhance the polymerization activity of supported Mo-based catalyst by reducing the molybdenum site from hexa-valent +6 into much lower valence state +2.

For a comparison with supported-MoO_x model catalysts, similar supported CrO_x/SiO₂ catalyst models with different Cr valence states (Cr⁵⁺, Cr⁴⁺, Cr³⁺ and Cr²⁺) were also established to find the optimal Cr oxidation state for ethylene polymerization. The SiO₂-supported chromium oxide models were designed according to **f** models (**5f**, **4f**, **3f** and **2f**) by simply substituting the molybdenum atom with chromium atom as shown in Table 3. The LANL2DZ basis set was used to describe the Cr element. The ground spin states of Cr⁵⁺, Cr⁴⁺, Cr³⁺ and Cr²⁺ centers were confirmed as doublet, triplet, quartet and quintet, respectively. Since ethylene could not coordinate with Cr⁵⁺ center model, Cr⁵⁺ center would not be the active site for ethylene polymerization. For the rest three chromium models, Cr³⁺ center possessed the lowest ethylene insertion energy barrier of 80.3 kJ/mol. Thus Cr³⁺ center was thought to be the most plausible oxidation state of active site for ethylene polymerization over Phillips CrO_x/SiO₂ catalyst. This is consistent with literature reports that +3 and +4 were the most generally accepted oxidation state for the active Cr site of ethylene polymerization corresponding to Cossee mechanism and metallacyclic mechanism, respectively [2]. It could be found that ethylene insertion energy barrier for Cr³⁺ center (80.3 kJ/mol) was much lower than that of Mo²⁺ polymerization center (e.g. ethylene insertion energy barrier for **2f** model was

Table 3Structures and ethylene insertion energy barrier for Cr active site models with different valence states supported on SiO₂ (energy in kJ/mol).

	Cr ⁵⁺	Cr ⁴⁺	Cr ³⁺	Cr ²⁺
Models				
Energy barrier	– ^a	87.8	80.3	95.3

^a Ethylene could not coordinate with Cr⁵⁺ active site, thus ethylene insertion energy barrier did not exist.

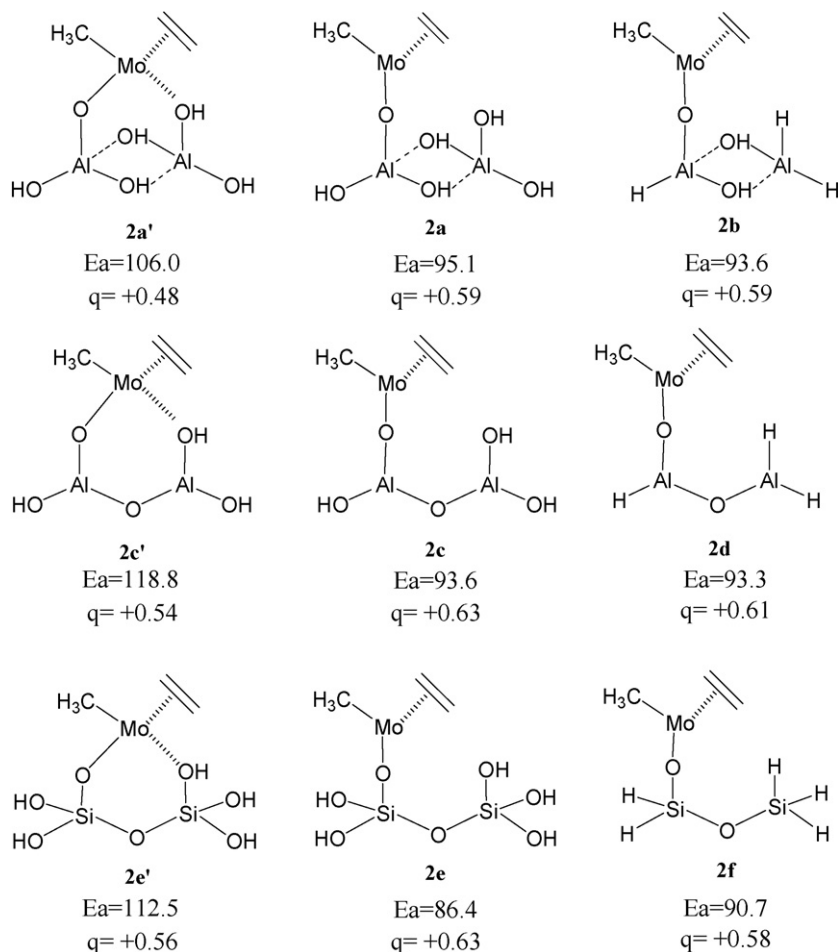
90.7 kJ/mol). This was in accordance with the experimental facts that ethylene polymerization activity of supported CrO_x Phillips catalyst was much higher than that of supported-MoO_x catalysts.

3.4. Effects of surface hydroxyl on the polymerization activity of Mo²⁺ centers

Surface hydroxyl on supports had been involved in many supported catalyst systems, such as metathesis [36], ethylene polymerization [37], etc. For olefin polymerization catalysts, hydroxyl group was usually considered as poison for active sites. In commercial polymerization process over Phillips catalyst [37], surface hydroxyl on support was always eliminated during catalyst preparation before olefin polymerization, e.g., by fluorination, calcination, to obtain highly active catalysts. But the specific mech-

anism has not been elucidated yet. Computational modeling was an efficient way to study the influence of surface hydroxyl on catalyst activity. Since the Mo²⁺ model possessed the lowest energy barrier, and may be the most plausible active site, further investigation would focus on the effects of surface hydroxyl on the activity of Mo²⁺ models (**2a**, **2b**, **2c**, **2d**, **2e** and **2f** models).

For **2a**, **2c** and **2e** models, the Mo–O distance about 3.0 Å between the hydroxyl and Mo atom indicated the non-coordination of hydroxyl on the divalent molybdenum centers. When hydroxyl was coordinated with molybdenum center with the Mo–O distance about 2.3 Å, three new catalyst models were obtained (named as **2a'**, **2c'** and **2e'** models, respectively). For **2b**, **2d** and **2f** models, there was only the non-coordination case because of the non-existence of hydroxyl on these three fully-dehydroxylated catalyst models.

**Fig. 6.** Ethylene insertion energy barrier (Ea, kJ/mol) and Mulliken charge (q) for Mo²⁺ centers with or without hydroxyl coordination.

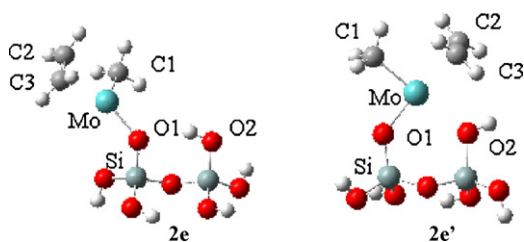


Fig. 7. Geometric optimized structures of **2e** (no hydroxyl coordination) and **2e'** (with hydroxyl coordination) models coordinated with C_2H_4 .

Fig. 6 shows the ethylene insertion energy barriers and Mulliken charges of Mo atom for **2a'**, **2c'**, **2e'**, **2a**, **2c** and **2e** models with or without coordination of hydroxyl on Mo centers. And their corresponding models with hydroxyl elimination (**2b**, **2d**, **2f**) were also listed for comparison. The ethylene insertion energy barrier for **2a'**, **2c'**, and **2e'** models with hydroxyl coordination were 106.0 kJ/mol, 118.8 kJ/mol, and 112.5 kJ/mol, respectively. When hydroxyl was not coordinated with Mo centers, the ethylene insertion energy barrier would decrease to 95.1 kJ/mol, 93.6 kJ/mol, and 86.4 kJ/mol for **2a**, **2c**, and **2e** models, respectively, which was very close to that of their corresponding models with hydroxyl elimination, such as 93.6 kJ/mol, 93.3 kJ/mol and 90.7 kJ/mol for **2b**, **2d**, and **2f** fully dehydroxylated models, respectively. It was demonstrated that the surface hydroxyl may poison the catalyst by coordination with the divalent molybdenum center. However, the non-coordination occasion would have little effect on the activity of the supported Mo-based catalysts.

The deactivation effect of hydroxyl coordination on Mo center for supported Mo-based catalyst might attribute to the electronic environment changes round molybdenum atom after hydroxyl coordination. As we all know, modification of CrO_x/SiO_2 catalyst with titanium [38] or fluorine [39] was always used in commercial industry to increase the electron deficiency of chromium center to improve the ethylene polymerization activity. Thus the catalyst activity for ethylene polymerization increased with the increase of electron deficiency of chromium center. In this work, as an electron donation group, the hydroxyl coordination on Mo center might increase the electron density and decrease the electron deficiency of Mo center, and thus decrease the catalyst activity. Take **2e** model as an example (its geometric structures with or without hydroxyl coordination are shown in Fig. 7). When hydroxyl was not coordinated with the Mo atom, the Mulliken charge of Mo was +0.63. When hydroxyl was coordinated with the Mo atom, the Mulliken charge of Mo atom would decrease to +0.56. Thus the coordination of hydroxyl could decrease the electron deficiency of Mo center and thus increase the ethylene insertion energy barrier. Up to now, the effect of surface hydroxyl group on the catalyst activity had been clearly understood. The theoretical results concerning the role of surface hydroxyl indicated that it is quite important to eliminate the surface residual hydroxyl groups during catalyst preparation in order to obtain highly active supported Mo-based catalyst for ethylene polymerization.

3.5. PIO study on the interaction between Mo^{2+} center and C_2H_4 monomer

PIO method was very powerful for analysis of the orbitals interaction and electronic transformation in catalytic reactions. As discussed above that ethylene insertion energy barrier for SiO_2 -supported catalysts were a little bit lower than that of the Al_2O_3 -supported ones and Mo center in the oxidation of +2 was thought to be the most plausible oxidation state of active site, thus **2f** model (defined as **A** fragment in PIO calculation) was selected, and the orbital interaction and electron transformation between **2f**

Table 4

Occupation number and overlap populations between **2f** model (**A**) and coordinated C_2H_4 monomer (**B**).

	PIOs	Occupation number			Overlap population
		A ^a	B ^a	Total	
Stationary state	PIO-1	1.65	0.44	2.10	0.15
	PIO-2	0.28	1.76	2.04	0.27
Transition state	PIO-1	1.45	0.82	2.26	0.26
	PIO-2	0.61	1.47	2.08	0.33

^a Fragment **A** is the **2f** center; Fragment **B** is C_2H_4 .

model and C_2H_4 monomer (defined as **B** fragment in PIO calculation) was investigated.

When ethylene inserted into **Mo–C1** bond, electron density accumulated in the regions between **C1** and **C2**, and between **Mo** and **C3**. It was preferable for ethylene insertion if the PIOs overlap in-phase in these bond regions, which would present a low energy barrier for ethylene insertion. So here, whether ethylene insertion process was easy or not could be judged by the in-phase overlaps in the regions between **C1** and **C2**, and between **Mo** and **C3**.

Twelve PIOs, from PIO-1 to PIO-12, were involved during **B** insertion into **A** center. But only the orbitals of PIO-1 and PIO-2 were considered due to their major contributions to the mutual orbital interaction. Contributions from other ten pairs of PIO orbitals were neglected. Table 4 lists the occupation numbers of electrons of PIO-1 and PIO-2 for the stationary state and transition state. It was shown that the overlap population of PIO-1 and the PIO-2 between **A** and **B** were all positive showing in-phase orbital overlap. The contour maps for PIO-1 and PIO-2 are shown in Fig. 8. So the **2f** center coordinated with ethylene was preferable for ethylene insertion. It was also noted that the occupation number of **A** was higher than that of **B** within PIO-1, and it was contrary for the case for PIO-2. Thus it was demonstrated that the PIO-1 showed the dominant delocalization of electron from **A** to **B** (back donation). However, the PIO-2 represented the delocalization of electron from **B** to **A** (donation). The molecular and atomic interaction between **A** and **B** in terms of molecular and atomic orbital interaction would be further studied as following.

As for **A** fragment, the molecular orbital number was 47, orbitals below the highest occupied molecular orbitals (HOMO) were defined as $HOMO_{-1(A)}$, $HOMO_{-2(A)}$, ... and the orbitals above the lowest unoccupied molecular orbitals (LUMO) were named as $LUMO_{+1(A)}$, $LUMO_{+2(A)}$, ... As for **B** part, the molecular orbital number was 12, and the six occupied orbitals and six unoccupied orbitals were defined as $HOMO_{(B)}$, $HOMO_{-1(B)}$, $HOMO_{-2(B)}$, ..., $HOMO_{-5(B)}$ and $LUMO_{(B)}$, $LUMO_{+1(B)}$, $LUMO_{+2(B)}$, ..., $LUMO_{+5(B)}$, respectively.

For the stationary state of **2f** model coordinated with ethylene, PIO-1 and PIO-2 results could be expressed in terms of linear combination of molecular orbital (LCMO) as shown in Eqs. (1)–(4). The PIO orbitals also could be expressed in terms of linear combination of atomic orbital (LCAO) as shown in Eqs. (5)–(8). The minor contributions were neglected. For the transition state of ethylene insertion on the **2f** model, their LCMO and LCAO were also expressed in Eqs. (9)–(16) as follows.

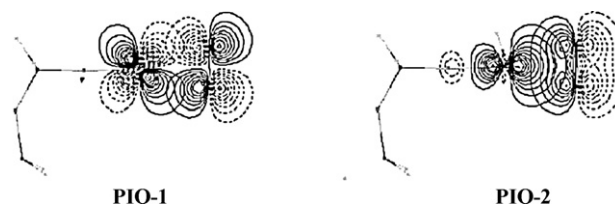


Fig. 8. Contour maps of PIO-1 and PIO-2 of **2f** model coordinated with C_2H_4 .

3.6. For stationary state

LCMO of PIO-1:

$$\text{PIO-1(A)} = 0.88\text{LUMO}_{(A)} + 0.44\text{HOMO}_{-1(A)} - 0.19\text{HOMO}_{(A)} + \dots \quad (1)$$

$$\text{PIO-1(B)} = 0.98\text{LUMO}_{(B)} - 0.2\text{HOMO}_{-4(B)} + \dots \quad (2)$$

LCMO of PIO-2:

$$\text{PIO-2(A)} = -0.79\text{LUMO}_{+2(A)} - 0.41\text{LUMO}_{+5(A)} + 0.22\text{HOMO}_{(A)} + \dots \quad (3)$$

$$\text{PIO-2(B)} = 0.97\text{HOMO}_{(B)} - 0.25\text{HOMO}_{-1(B)} + \dots \quad (4)$$

LCAO of PIO-1:

$$\text{PIO-1(A)} = 0.68\text{Mo}4d_{xy} - 0.65\text{Mo}4d_{x^2-y^2} + \dots \quad (5)$$

$$\text{PIO-1(B)} = 0.75\text{C}(1)2p_x - 0.72\text{C}(2)2p_x + \dots \quad (6)$$

LCAO of PIO-2:

$$\text{PIO-2(A)} = -0.49\text{Mo}4d_{z^2} + 0.45\text{Mo}5s + 0.40\text{Mo}4d_{xy} + \dots \quad (7)$$

$$\text{PIO-2(B)} = -0.58\text{C}(1)2p_x - 0.57\text{C}(2)2p_x + \dots \quad (8)$$

3.7. For transition state

LCMO of PIO-1:

$$\text{PIO-1(A)} = +0.75\text{HOMO}_{-2(A)} - 0.45\text{HOMO}_{-1(A)} + 0.27\text{LUMO}_{+2(A)} + \dots \quad (9)$$

$$\text{PIO-1(B)} = -0.94\text{LUMO}_{(B)} + 0.27\text{HOMO}_{-4(B)} + \dots \quad (10)$$

LCMO of PIO-2:

$$\text{PIO-2(A)} = -0.64\text{LUMO}_{+1(A)} - 0.56\text{LUMO}_{+2(A)} + 0.46\text{HOMO}_{-2(A)} + \dots \quad (11)$$

$$\text{PIO-2(B)} = 0.98\text{HOMO}_{(B)} - 0.12\text{LUMO}_{(B)} + \dots \quad (12)$$

LCAO of PIO-1:

$$\text{PIO-1(A)} = -0.48\text{Mo}4d_{yz} + 0.37\text{Mo}4d_{x^2-y^2} + \dots \quad (13)$$

$$\text{PIO-1(B)} = 0.49\text{C}(1)2p_y - 0.48\text{C}(1)2p_x + \dots \quad (14)$$

LCAO of PIO-2:

$$\text{PIO-2(A)} = -0.44\text{Mo}4d_{zx} + 0.43\text{Mo}5s + \dots \quad (15)$$

$$\text{PIO-2(B)} = -0.50\text{C}(2)2p_y - 0.47\text{C}(2)2p_z + \dots \quad (16)$$

From the LCMO results for stationary state, the main components of PIO-1 between **A** and **B** were observed as $\text{LUMO}_{(A)}$, $\text{HOMO}_{-1(A)}$, $\text{LUMO}_{(B)}$, respectively. And the main components of PIO-2 included $\text{LUMO}_{+2(A)}$, $\text{HOMO}_{(B)}$. It was demonstrated that the interactions occurred between the occupied molecular orbital of both **A** and **B**. The LCAO expression showed that the important components of atomic orbitals between **A** and **B** could be contributed mainly from $\text{Mo}4d_{xy}$, $\text{Mo}4d_{x^2-y^2}$, and $\text{C}2p_x$ for PIO-1, and $\text{Mo}4d_{z^2}$, $\text{Mo}5s$, $\text{Mo}4d_{xy}$ and $\text{C}2p_x$ for PIO-2.

The result of LCMO and LCAO for transition state showed that the main components of PIO-1 between **A** and **B** were $\text{HOMO}_{-2(A)}$, $\text{LUMO}_{(B)}$, respectively, and mainly contributed from atomic orbitals $\text{Mo}4d_{yz}$, $\text{C}2p_x$, and $\text{C}2p_y$. These interactions occurred between the occupied orbitals of **A** and the unoccupied orbitals of **B**. The main components of PIO-2 were $\text{LUMO}_{+1(A)}$ and $\text{HOMO}_{(B)}$, mainly contributed from atomic orbitals $\text{Mo}4d_{zx}$, $\text{C}2p_y$, and $\text{C}2p_z$. These

interactions occurred between the unoccupied orbitals of **A** and the occupied orbitals of **B**. Thus the dominant electron transfer would be from **A** to **B** in PIO-1, and electron transfer would be from **B** to **A** in PIO-2.

In additionally, the overlaps populations of the PIO-1 and PIO-2 in the transition state were obviously higher than the corresponding values of the stationary state (shown in Table 4), which meant more advanced electron delocalization in the transition states than in the coordinated state.

In summary, the obtained PIO results indicated that the overlap of PIO-1 and PIO-2 for **2f** center and C_2H_4 monomer was in-phase. The dominant electron transformation was from **2f** center to C_2H_4 monomer for PIO-1 and from C_2H_4 monomer to **2f** center for PIO-2. The molecular orbital interaction during ethylene coordination and insertion had been elucidated in terms of specific LCMO and LCAO contributions.

4. Conclusion

$\text{MoO}_x/\text{Al}_2\text{O}_3$ and $\text{MoO}_x/\text{SiO}_2$ catalysts were all active for ethylene polymerization with relatively low activity. In order to develop new supported molybdenum oxides catalyst with high performance, their corresponding catalyst models had been established to investigate the effects of molybdenum valence state and surface hydroxyl on catalyst activity by the combination of DFT and PIO methods. DFT results showed that ethylene insertion energy barrier for SiO_2 -supported catalysts were a little bit lower than the alumina-supported ones. For the same kind of support, Mo^{2+} center presented the lowest energy barrier of ethylene insertion, while Mo^{4+} center possessed the highest energy barrier. PIO results showed that the overlaps between Mo^{2+} center and ethylene were in-phase for PIO-1 and PIO-2, which was preferable for ethylene insertion into Mo–C single bond, and the dominant electron transformation was from Mo^{2+} center to ethylene for PIO-1, and from ethylene to Mo^{2+} center for PIO-2. The molecular orbital interaction during ethylene coordination and insertion had been elucidated in terms of specific LCMO and LCAO contributions. In addition, the coordination of hydroxyl with Mo center could decrease the electron deficiency of molybdenum center, thus increase the ethylene insertion energy barrier. But the non-coordination of hydroxyl on active site had little effect on catalyst activity. It had been demonstrated that pre-reduction of hexa-valent Mo into lower valence state +2 and elimination of surface hydroxyl groups during catalyst preparation were the key factors to obtain highly efficient Mo-based catalysts for ethylene polymerization. The molecular modeling results obtained in this work could provide good theoretical basis for further exploration of green and highly efficient Mo-based supported polyethylene catalysts, so that the highly toxic Phillips Cr-based catalyst could be finally substituted in the future.

Acknowledgements

We gratefully thank the financial support by Shanghai Municipal Education Commission (Key Project of Innovation 2008). This work is also financially supported by the research program of the State Key Laboratory of Chemical Engineering, Shanghai Pujiang Talent Plan Project (08PJ14032) and the Program of Introducing Talents of Discipline to Universities (B08021).

Appendix A. Supplementary data

Supplementary data associated with this article can be found, in the online version, at doi:10.1016/j.molcata.2010.01.018.

References

- [1] T.J. Pullukat, R.E. Hoff, *Catal. Rev. Sci. Eng.* 41 (1999) 389.
- [2] M.P. McDaniel, *Adv. Catal.* 33 (1985) 47.
- [3] A.B. Gaspar, L.C. Dieguez, *Appl. Catal. A: Gen.* 227 (2002) 241.
- [4] V.J. Ruddick, J.P.S. Badyal, *Langmuir* 13 (1997) 469.
- [5] V.J. Ruddick, J.P.S. Badyal, *J. Phys. Chem. B* 101 (1997) 9240.
- [6] H.R. Sailors, J.P. Hogan, *J. Macromol. Sci. Chem. A* 15 (1981) 1375.
- [7] E. Field, M. Feller, US2731452 (1956).
- [8] A.M. Rouhi, *Chem. Eng. News* 80 (2002) 29.
- [9] S.L. Liu, S.J. Huang, W.J. Xin, J. Bai, S.J. Xie, L.Y. Xu, *Catal. Today* 93–95 (2004) 471.
- [10] J.C. Mol, *J. Mol. Catal. A: Chem.* 213 (2004) 39.
- [11] X.J. Li, W.P. Zhang, S.L. Liu, L.Y. Xu, X.W. Han, X.H. Bao, *J. Phys. Chem. C* 112 (2008) 5955.
- [12] X.J. Li, W.P. Zhang, S.L. Liu, S.J. Xie, X.X. Zhu, X.H. Bao, L.Y. Xu, *J. Mol. Catal. A: Chem.* 313 (2009) 38.
- [13] J. Guan, G. Yang, D.H. Zhou, W.P. Zhang, X.C. Liu, X.W. Han, X.H. Bao, *J. Mol. Catal. A: Chem.* 300 (2009) 41.
- [14] J. Handzlik, J. Ogonowski, *J. Mol. Catal. A: Chem.* 175 (2001) 215.
- [15] H. Fujimoto, N. Koga, I. Hataue, *J. Phys. Chem.* 88 (1984) 3539.
- [16] K. Fukui, T. Yonezawa, H. Shingu, *J. Chem. Phys.* 20 (1952) 722.
- [17] J. Handzlik, A. Shiga, J. Kondziolka, *J. Mol. Catal. A: Chem.* 284 (2008) 8.
- [18] A. Shiga, H. Kawamura-Kuribayashi, T. Sasaki, *J. Mol. Catal.* 77 (1992) 135.
- [19] B. Liu, Y.W. Fang, M. Terano, *Mol. Simul.* 30 (2004) 963.
- [20] M.J. Frisch, G.W. Trucks, H.B. Schlegel, G.E. Scuseria, M.A. Robb, J.R. Cheeseman, J.A. Montgomery Jr., T. Vreven, K.N. Kudin, J.C. Burant, J.M. Millam, S.S. Iyengar, J. Tomasi, V. Barone, B. Mennucci, M. Cossi, G. Scalmani, N. Rega, G.A. Petersson, H. Nakatsuji, M. Hada, M. Ehara, K. Toyota, R. Fukuda, J. Hasegawa, M. Ishida, T. Nakajima, Y. Honda, O. Kitao, H. Nakai, M. Klene, X. Li, J.E. Knox, H.P. Hratchian, J.B. Cross, V. Bakken, C. Adamo, J. Jaramillo, R. Gomperts, R.E. Stratmann, O. Yazyev, A.J. Austin, R. Cammi, C. Pomelli, J.W. Ochterski, P.Y. Ayala, K. Morokuma, G.A. Voth, P. Salvador, J.J. Dannenberg, V.G. Zakrzewski, S. Dapprich, A.D. Daniels, M.C. Strain, O. Farkas, D.K. Malick, A.D. Rabuck, K. Raghavachari, J.B. Foresman, J.V. Ortiz, Q. Cui, A.G. Baboul, S. Clifford, J. Cioslowski, B.B. Stefanov, G. Liu, A. Liashenko, P. Piskorz, I. Komaromi, R.L. Martin, D.J. Fox, T. Keith, M.A. Al-Laham, C.Y. Peng, A. Nanayakkara, M. Challacombe, P.M.W. Gill, B. Johnson, W. Chen, M.W. Wong, C. Gonzalez, J.A. Pople, *Gaussian 03*, Revision E.01, Gaussian, Inc., Wallingford, CT, 2004.
- [21] A.D. Becke, *J. Chem. Phys.* (1993) 5648.
- [22] A.D. Becke, *Phys. Rev. A* 38 (1988) 3098.
- [23] C. Lee, W. Yang, R.G. Parr, *Phys. Rev. B* 37 (1988) 785.
- [24] C. Gonzalez, H.B. Schlegel, *J. Chem. Phys.* 90 (1989) 2154.
- [25] C. Gonzalez, H.B. Schlegel, *J. Phys. Chem.* 94 (1990) 5523.
- [26] P.J. Hay, W.R. Wadt, *J. Chem. Phys.* 82 (1985) 299.
- [27] J.L.G. Fierro, H. Heinemann, *Metal Oxides: Chemistry and Applications*, FL: Taylor & Francis, Boca Raton, 2005.
- [28] P. Cossee, *J. Catal.* 3 (1964) 80.
- [29] T. Monoi, Y. Sasaki, *J. Mol. Catal. A: Chem.* 187 (2002) 135.
- [30] H. Ikeda, T. Monoi, Y. Sasaki, *J. Polym. Sci. Part A: Polym. Chem.* 41 (2003) 413.
- [31] R. Radhakrishnan, C. Reed, S.T. Oyama, M. Seman, J.N. Kondo, K. Domen, Y. Ohminami, K. Asakura, *J. Phys. Chem. B* 105 (2001) 8519.
- [32] J. Handzlik, *J. Mol. Catal. A: Chem.* 218 (2004) 91.
- [33] G. Hierl, H.L. Krauss, *Z. Anorg. Allg. Chem.* 415 (1975) 57.
- [34] Ø. Espelid, K.J. Bøve, *J. Catal.* 195 (2000) 125.
- [35] C.A. Demmelmaier, R.E. White, J.A. van Bokhoven, S.L. Scott, *J. Catal.* 262 (2009) 44.
- [36] E. Groppo, C. Lamberti, S. Bordiga, G. Spoto, A. Zecchina, *Chem. Rev.* 105 (2005) 115.
- [37] S.M. Augustine, J.P. Blitz, *J. Catal.* 161 (1996) 641.
- [38] A. Ellison, T.L. Overton, *J. Mol. Catal. A: Chem.* 90 (1994) 81.
- [39] B. Adamczyk, O. Boese, N. Weiher, S.L.M. Schroeder, E. Kemnitz, *J. Fluorine Chem.* 101 (2000) 239.